4

Axial segregation in metal-halide lamps under gravity conditions ranging from 1 to 10 g

Abstract. Axial segregation in metal-halide lamps is caused by a complex interaction between convection and diffusion and is not yet fully understood. By enhancing convection, by placing the lamp in a centrifuge, the effect of convection on axial segregation was studied. The centrifuge caused the lamp to be accelerated between 1 and 10 g. Optical emission spectroscopy was performed on a metal-halide lamp while placed in the centrifuge. Several transitions of atomic and ionic Dy, and atomic Hg have been measured at different lateral positions from which we obtained atomic and ionic Dy and atomic Hg intensity profiles. Atomic lateral profiles of Dy at different axial positions in the lamp were used for the calculation of Fischer's axial segregation parameter. The theoretical model of the Fischer curve, which shows the axial segregation parameter as a function of convection, was verified along the full range by measuring lamps of different filling and geometry. Moreover, the radial temperature profile of the arc for the different accelerations was determined.

Journal of Physics D 40, 2839, 2007.

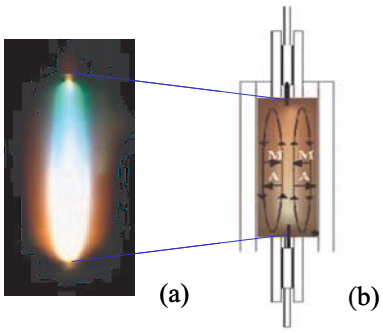

Figure 4.1: (a) Colour separation in a metal-halide lamp burner. (b) Schematic view of a metal-halide lamp; diffusion and convection of atoms (A) and molecules (M) are indicated by arrows. See figure 1.1 for full colour.

4.1 Introduction

The wish for compact high-intensity light sources with high luminous efficacy and good colour rendering properties has led to the development of the metal-halide lamp [1]. This type of arc lamp contains a buffer gas of Hg and a relatively small amount of a mixture of metal-halide additives such as DyI_3, CeI_3 or NaI salts, which supply the prime radiators. At least two salt components are necessary for a good colour rendering index, therefore mixtures such as (NaI + ScI_3), (NaI + TlI +InI) or (NaI + TlI + DyI_3 +HoI_3 + TmI_3) are commonly used in metal-halide lamps.

Due to the competition between diffusive and convective processes these additives are non-uniformly distributed over the lamp, resulting in the undesirable segregation of colours [2], see figure 4.1. Since the convective processes are induced by gravity, excluding or increasing the effects of gravity on the arc allows for a better understanding of the segregation phenomenon in the metal-halide lamp. During experiments at the international space station (ISS) the lamp operated under micro-gravity conditions [3], thereby eliminating the convective processes in the arc.

Both micro and hyper-gravity conditions were obtained during parabolic flights [4] [5] where micro-gravity and hyper-gravity up to $2g$ was obtained for 20 to 25 seconds. More time, however, is needed for the arc to stabilize. Also, it would be of interest to subject the lamp to g's higher than 2. Therefore, a centrifuge was built that allows for an acceleration ranging from 1 to $10g$. In the centrifuge the lamps were subjected to extended hyper-gravity conditions in order to separate and help clarify the role of convection and other transport mechanisms in the arc of the lamp. For the purpose of this study the lamp was filled with an Hg buffer gas and one salt, namely DyI_3. In this way a relatively simple salt system was achieved allowing for the experimental results to be easily compared with the results of numerical modelling. The lamp was investigated by means of optical emission spectroscopy, which yields line intensities of the species Hg and Dy [6]. From calibrated Hg line intensities we constructed radial temperature profiles.

This chapter is organized as follows. Section 4.2 describes the segregation phenomenon and the method used to determine the temperature of the arc. Section 4.3 describes the arc lamps used in the experiments and the experimental setup. Results from the experiments are presented and discussed in section 4.4. These results constitute lateral intensity profiles at different axial positions, the axial segregation parameter as a function of g and radial profiles of the arc temperature. Finally, section 4.5 offers conclusions and recommendations for future work.

4.2 Theory

4.2.1 Segregation

The main light emitting species, Dy atoms and ions, are brought into the plasma by evaporation of the liquid DyI_3, these Dy molecules dissociate into atoms and ions. Whereas the Hg evaporates completely, only a fraction of the few milligrams of the DyI_3 additive evaporates. The rest of the DyI_3 remains as a liquid salt pool at the coldest spot of the burner wall. The cold spot determines the vapour pressure of the additive in the immediate vicinity of the salt pool. Because of the large temperature gradient between the wall ($\sim$ 1200 K) and the centre of the burner ($\sim$ 6000 K) [7], a multi-step dissociation process of DyI_3 molecules towards the centre and association of atoms into molecules near the wall takes place. The chain of reaction balances can be described as follows,

$$\mathrm{DyI_3} \rightleftarrows \mathrm{DyI_2} + \mathrm{I} \rightleftarrows \mathrm{DyI} + 2\mathrm{I} \rightleftarrows \mathrm{Dy} + 3\mathrm{I}, \tag{4.1}$$

where the temperature increases to the right. At the hot centre Dy atoms ionize and Dy ions are created,

$$\mathrm{Dy} + e \rightleftarrows \mathrm{Dy^+} + e + e. \tag{4.2}$$

Three mechanisms influence the distribution of particles in the plasma. First, there is a high temperature in the centre, which rapidly decreases towards the wall. Because of $p = nkT$ this high temperature results in a hollow profile of the density distribution over the lamp. Second, there is the difference between the diffusion velocities of atoms and molecules. The smaller and lighter Dy atoms diffuse faster outward than the larger and heavier molecules (DyI, DyI_2, DyI_3) diffuse inward. This difference in diffusion velocity results, in steady-state, in an even more hollow profile of the elemental density of Dy. This phenomenon is called radial segregation [2]. Elemental density is defined as the density that contains all molecular, atomic and ionic contributions of a particular element. For example, for Dy the elemental density (denoted with {}) can be described as

$$\{n_{Dy}\} = [Dy] + [Dy^+] + [DyI] + [DyI_2] + [DyI_3]. \tag{4.3}$$

The third mechanism, convection, causes the hot gas to move upwards in the hot centre of the arc and downwards along the cool wall of the lamp. This movement of the bulk gas drags the high concentration of Dy near the wall downwards. Moreover, the lower

concentration of Dy in the centre, caused by the radial segregation, is dragged upwards. As a consequence, high density of elemental Dy accumulates at the bottom of the arc, a phenomenon which is known as axial segregation [2]. The combination of axial and radial segregation is shown in figure 4.1(b).

4.2.2 Axial segregation

Fischer theoretically described the diffusion-convection mechanism for axial segregation in vertically operated lamps [2]. In his model of axial segregation of additives of metal-halide lamps he assumed that the arc temperature profile is parabolic and independent of axial position. The convection profile (which is governed completely by the buffer gas in all metal-halide lamps) can be calculated using the Navier-Stokes equation:

$$\frac{\partial p}{\partial z} + \rho_m \tilde{g} - \frac{1}{r}\frac{\partial}{\partial r}\left(r\eta\frac{\partial v_z}{\partial r}\right) = 0 \tag{4.4}$$

with the boundary conditions

$$\frac{\partial v_z}{\partial r}|_{r=0} \qquad v_z = 0|_{r=R} \tag{4.5}$$

where r is the radial position, R the radius of the arc tube, ρ_m the buffer gas mass density, η the viscosity of the buffer gas, v_z the axial velocity (the radial velocity is assumed to be zero) and $\tilde{g}$ the acceleration. Normally, $\tilde{g}$ stands for gravitational acceleration, in this case this stands for the acceleration caused by the centrifuge. In this paper the amount of acceleration is given in terms of $g = 9.8m/s^2$. The axial velocity can be described as [16]

$$v_z \sim \frac{p_{Hg} R^2 \tilde{g}}{\eta} \tag{4.6}$$

This equation shows that the axial velocity, which equals the convection speed, is proportional to the acceleration $\tilde{g}$. The axial segregation can therefore be directly influenced by $\tilde{g}$.

Fischer described axial segregation by showing that the density declines along the axis exponentially [2]

$$n_i(z) = n_{i,0} \exp(-\lambda z), \tag{4.7}$$

where λ is the axial segregation parameter for species i, z the height and $n_{i,0}$ the density at the bottom of the arc. There are two extreme cases. At high values for the buffer gas pressure p_0, burner radius R and g the axial segregation parameter can be approximated by

$$\lambda \approx p_0^2 R^2 g \tag{4.8}$$

and for low values of the buffer-gas pressure, burner radius and g by

$$\lambda \approx (p_0^2 R^2 g)^{-1} \tag{4.9}$$

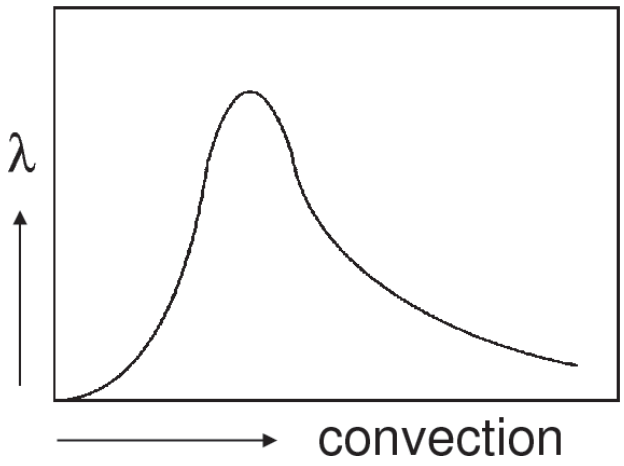

Figure 4.2: The Fischer curve [2] which represents the dependence of the axial segregation parameter λ on convection, or g.

The region in-between has a maximum, see figure 4.2. This curve that shows the axial segregation parameter λ as a function of convection is called the Fischer curve. On the left-hand side λ increases as a function of g and therefore as a function of convection. On the right-hand side λ decreases as a function of convection. By placing the lamp in a centrifuge and by using lamps with a different buffer gas pressure the full curve can be covered experimentally.

4.2.3 Emission of radiation

One way to study the effect of radial and axial segregation is to determine the radial density profiles of the additives. If the discharge is in LTE (Local Thermodynamic Equilibrium) [8], the density of the additives can be determined by measuring the intensity of light emitted by atoms and ions.

For an optically thin line, the radiant power $U_{pq}(\mathrm{r})$ [Wm^{-3}] emitted by a spectral line is

$$U_{pq}(r) = A(p,q)h\nu_{pq}n_{\mathrm{p}}, \tag{4.10}$$

where $A(p,q)$ is the transition probability of the transition between the upper energy level p and the lower level q, $h\nu_{pq}$ the energy of the emitted photon, and n_{p} the number density of an emitting atom or ion in upper energy level p.

The radiant power $U_{pq}(\mathrm{r})$ of an optically thin line is deduced from the lateral (i.e. line-of-sight) measurement of the arc. First the spectral intensity $I_\lambda(\lambda, x)$ is measured as a function of lateral position x and calibrated with a ribbon lamp with known spectral intensity. Then these absolute spectral intensities are subsequently integrated over the transition giving $I_{pq}(x)$. The integrated spectral line intensity $I_{pq}(x)$ as a function of lateral position x is called the lateral profile. Finally, radial information can be extracted from the lateral profile by the Abel inversion technique [9]. Abel inversion of $I_{pq}(x)$ gives the transition

integrated emission coefficient $j_{pq} = A(p,q)h\nu_{pq}n_p/(4\pi)$ from which $U_{pq}(\mathrm{r}) = A(p,q)h\nu_{pq}n_p$ can be determined.

Once $U_{pq}(\mathrm{r})$ is known the radial temperature profile can be calculated from the dominant species, in this case atomic Hg [3, 10]. Rewriting equation 4.10 using $n_p = n_{total}\ g_p \exp(-E_\mathrm{p}/kT)/Q(T)$ [11], the temperature can be calculated from the following equation

$$n_{Hg} = \frac{U_{pq}(r)Q(T)}{g_\mathrm{p}A(p,q)h\nu_{pq}} \exp\left(\frac{E_\mathrm{p}}{kT}\right), \tag{4.11}$$

where n_{Hg} is the total number (system) density of particles of atomic Hg, $U_{pq}(\mathrm{r})$ is determined experimentally, while the partition function $Q(T)$, g_p, $A(p,q)$ can be found in literature [12] [13] [14]. $U_{pq}(\mathrm{r})$ is determined from the calibrated optically thin 579 nm Hg line. The total Hg density n_Hg can be reformulated in terms of temperature using the ideal gas law $p = nkT$, assuming that $p = p_\mathrm{Hg}$ and that the pressure is constant over the discharge, where p_Hg can be written as

$$p_{Hg} = n_\mathrm{Hg}\ kT_{eff} = \frac{N_{Hg}kT_\mathrm{eff}}{V} = \frac{m_\mathrm{effHg}N_A kT_\mathrm{eff}}{m_\mathrm{Hg}\pi R^2 h}. \tag{4.12}$$

N_A is Avogadro's number, m_{Hg} the molar mass of Hg; and R and h the total radius and length of the burner respectively. N_{Hg} is the total amount of Hg in the discharge region, T_{eff} the effective temperature and m_{effHg} the total Hg dose in the discharge region. Assuming cylinder symmetry, the effective temperature T_{eff} can be written as [3]

$$T_\mathrm{eff} = \frac{R^2}{2\int_0^R \frac{r}{T(r)}dr}. \tag{4.13}$$

Combined with equation (4.11), $T(r)$ can be calculated numerically from the measured $U_p(\mathrm{r})$ of the 579 Hg line using an iterative method [3].

The 579 nm Hg line cannot, however, be accurately determined at radial positions beyond $r > 2$ mm. Therefore, the temperature profile is extrapolated using the expression for the radial temperature profile introduced by Fischer [15]

$$T(r) = T_{wall} + T_1\left(1 - \left(\frac{r}{R}\right)^2\right) + T_2\left(1 - \left(\frac{r}{R}\right)^2\right)^\gamma, \tag{4.14}$$

with r the radial position and R the total radius of the arc tube, γ is a measure for the amount of contraction of the discharge. Equation 4.14 is used to extrapolate the temperature from the inner part of the burner to the wall. In most HID lamps, the discharge contracts toward the axis of the arc tube, creating a dark annular space between the discharge and the tube wall [16]. The gas temperature profile in such a contracted discharge can be described by an expression proposed by Fischer for high pressure discharges [3, 15] T_1 and T_2 are fitting parameters that determine the maximum temperature in the centre of the discharge (r=0), together with the value of γ. The wall temperature T_wall is measured to be about 1200 K at the midplane of the lamp [7] that was investigated in this study. The error in the temperature profile is estimated to be less than 10% over the whole range.

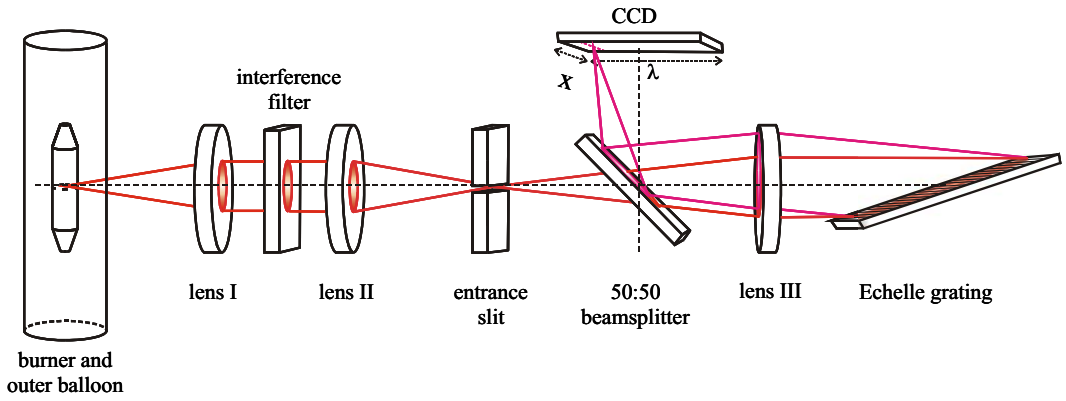

Figure 4.3: Setup [3, 10] used for both the ISS and centrifuge measurements. It is an Echelle type spectrometer in Littrow configuration, the imaging lens (III) is used for the collimation of both the un-dispersed beam of light as well as the reflected dispersed beam of light.

4.3 Experimental Setup

The spectrometer is attached to the arm of a centrifuge, see figure 4.4. The arm is 1.0 m long and the centrifuge is about 2 m high. The maximum speed is 13.8 m/s, when this is reached the resultant acceleration, that is parallel to the lamp axis, equals 10 g. A schematic representation of the acceleration of the lamp is shown in figure 4.5.

The design for the spectrometer used for the optical emission measurements of HID lamps, was at first used for measurements in the ISS [3]. As the spectrometer had to be compact, light weight, and robust, it was an ideal design for the spectrometer on the centrifuge.

A schematic of the Echelle-type spectrometer is shown in figure 4.3 [3, 10]. The light originating from the plasma forms a parallel beam after going through lens I (100 mm focal distance). A parallel beam is necessary for the proper functioning of the wavelength selection by the interference filter, which is situated between lens I and lens II (also 100 mm focal distance). Lens I and II combined with the interference filter form a 1:1 image of the burner on the horizontally placed entrance slit (10 mm x 10 μm) of the desired wavelength interval. The light emanating from the slit is the emission along the lateral cross-section at one axial position of the burner. It passes a 50:50 beam splitter and after being collimated by an achromatic doublet (Lens III), the light reaches the Echelle grating (96 mm x 46 mm) having 79.01 lines/mm and a 74.1° blaze angle. Lens III is positioned at its focal distance (150 mm) from the entrance slit to create a parallel beam of light on the Echelle grating. Then the light is back-reflected and dispersed with conservation of the spatial information. The angle of the reflected light with the optical axis of the system depends on the wavelength of the light. The reflected light is collimated by the same doublet (Lens III) and focused via the 50:50 beam splitter on the CCD-surface of the camera (SBIG ST-2000XM, 1600x1200 pixels of 7.4μm x 7.4 μm). As the wavelength dispersion is imaged in the horizontal direction and the lateral position in the vertical, we obtain a complete

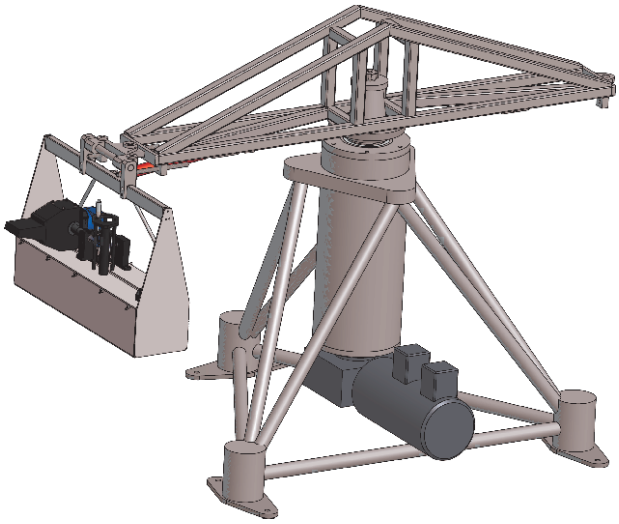

Figure 4.4: The centrifuge with the spectrometer attached to the arm.

lateral profile in one measurement. The two-dimensional CCD image therefore contains, in the vertical direction, the lateral cross-section of the lamp, measured at one axial position. Moving the lamp vertically allows for measurements at different axial positions. In the horizontal direction the CCD image contains the wavelengths of different atomic and ionic transitions. A broad wavelength selection is done by selecting the interference filter that corresponds to the desired wavelength interval [3].

All lines were calibrated, using a ribbon lamp that was placed at exactly the same position as the metal-halide lamp in the centrifuge setup.

species	**line (nm)**	**A value**	**source A value**
Dy I	642.19	1.6×10^{5} s^{-1}	Kurucz [12]
Dy II	402.44	8.4×10^{6} s^{-1}	Wickliffe and Lawler [13]
Hg I	579.07	2.1×10^{7} s^{-1}	Derived from Benck and Lawler [17]

Table 4.1: Lines measured with the Echelle spectrometer. The A value for the 579.07 nm Hg line is derived from the $g_{\mathrm{p}}A$ value for the 576.96 nm line [3, 17].

In the centrifuge experiment, emission spectroscopy was performed on a metal-halide lamp [18, 19]. The lamp consists of a quartz burner of 20 mm in length and 8 mm in inner diameter and a transparent quartz vacuum outer bulb. Measurements were also performed on a lamp of 22 mm length and 4 mm diameter. The burner is made of quartz in order to make the arc optically accessible. It is driven by a Luxmate Dimtronics 150 ballast with a 120 Hz square wave voltage.

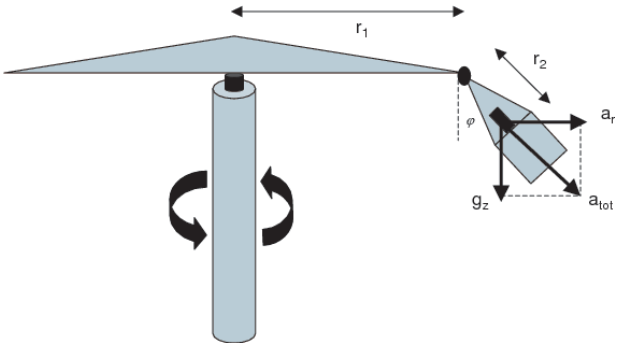

Figure 4.5: Schematic representation of the acceleration applied to the lamp when the centrifuge is spinning. a_r is the centrifugal acceleration, g_z the gravitational acceleration and a_{tot} is the resultant acceleration which is expressed in terms of g.

4.4 Results and discussion

The vertically burned lamps were subjected to an acceleration from 1 to 10 g, during which the emission spectroscopy measurements were done. The lamp was also monitored with a webcam, figure 4.6 shows webcam images for a lamp containing 5 mg Hg and 4 mg DyI_3. These images clearly show how the blueish-white light, caused by Dy atoms, is being more evenly distributed over the lamp as g becomes higher. As is typical for a lamp on the right side of the Fischer curve, this is caused by the mixing which is increased as the convection is increased, leading to a decrease in axial segregation. It needs to be mentioned that although the webcam causes the actual colours to distort, this does not hinder qualitative analysis.

This is also apparent when we look at the lateral profiles constructed at different axial positions in the lamp of atomic Dy, see figure 4.7, and of ionic Dy, see figure 4.8. Figures 4.7 and 4.8 show the lateral profiles near the bottom, the centre and near the top of the lamp containing 10 mg Hg and 4 mg DyI_3. As expected the ion density is highest on the axis of the central region of the arc, while a dip in the radial distribution of the Dy atoms is found. From the lateral profile near the bottom, we see that at higher g-values the amount of Dy atoms and ions decline, whereas at the top the amount of Dy atoms and ions increase as g increases.

The decrease of Dy near the bottom at higher g could be caused by the decrease of the cold spot temperature as g is increased. This can happen in two ways. First, as g is increased, convection increases, causing the arc to contract. Contraction of the arc means that the surrounding wall becomes cooler, this causes the cold spot temperature to decrease, thereby releasing less Dy into the arc. This contraction can also be seen in figures 4.7(a) and 4.8 (a) at higher g. Second, the power is being distributed more evenly over the arc as Dy is being more mixed, therefore the reduced power density at the bottom causes the cold spot temperature to decline. It needs to be mentioned that when comparing the lateral profiles at the top and the bottom of the lamp, there is always more Dy at the

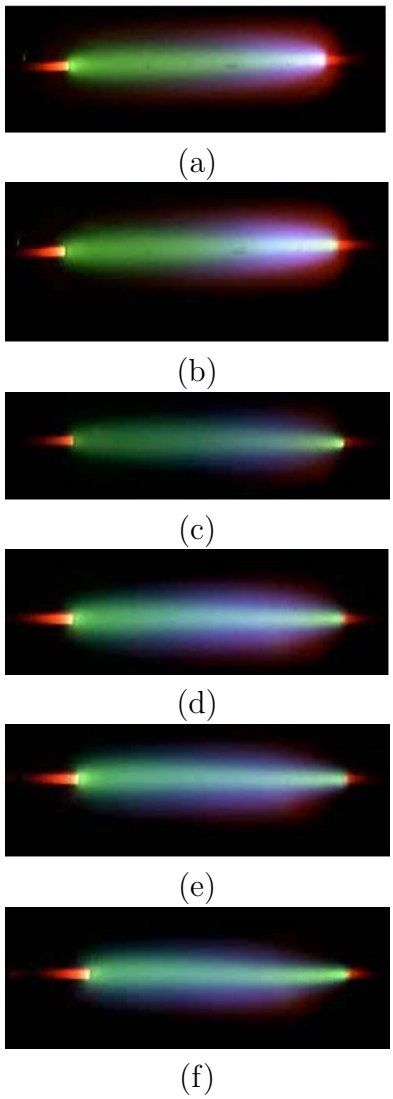

Figure 4.6: Webcam images for a lamp containing 5 mg Hg and 4 mg DyI_3. Figure (a) is the lamp at $1g$, (b) at $2g$, (c) at $4g$, (d) at $6g$, (e) at $8g$ and (f) at $10g$. The lamp was burned vertically, this means the acceleration coincides with the central axis, the bottom of the lamp is on the right-hand side of the images.

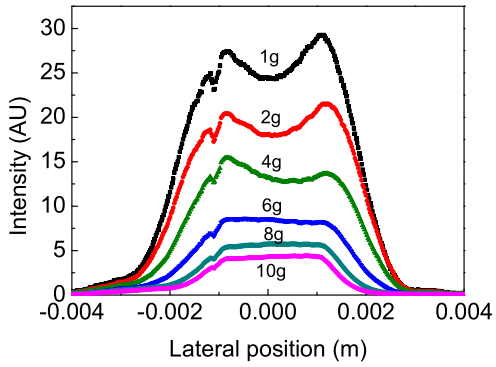

(a)

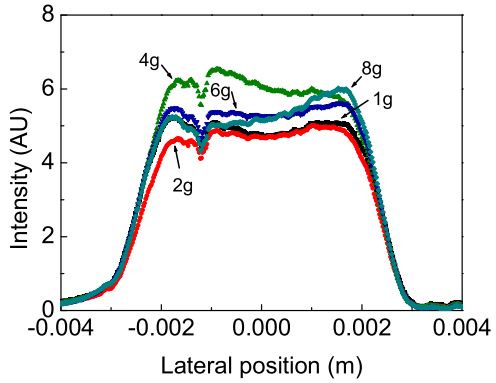

(b)

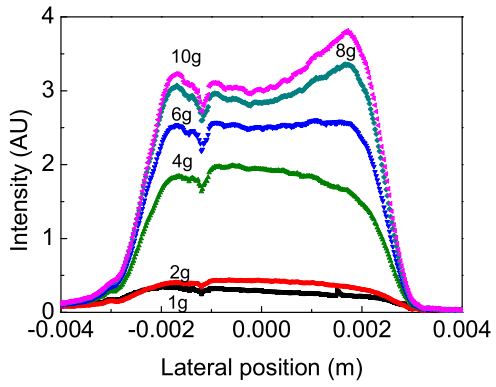

(c)

Figure 4.7: Atomic lateral profiles for the atomic Dy line at 642.19 nm. The lamp filling was 10 mg Hg and 4 mg DyI_3, the measurements were done at three different axial positions z, (a) near the bottom at z/Z=27,5% (b) at the centre at z/Z=50% (c) near the top at z/Z=72.5% where Z=20mm. Although the intensity was not calibrated, the measurements done at the same wavelength are absolute with respect to each other.

bottom than at the top, so the axial segregation remains.

Near the top of the lamp it is clear that for higher g-values more Dy atoms reach the top of the lamp. Figure 4.7(c) shows that there is no change in contraction and figure 4.8(c) shows in fact that there is a broadening of the arc.

The axial segregation parameter λ can be calculated in different ways, either using the radial density or the lateral intensity as a function of axial position. Both of these were examined as a function of g, yielding the Fischer curve, this is shown in figure 4.9. The curves are identical within the error margin and shows the same shape as figure 4.2. Apparently it does not matter whether the radially resolved density or the lateral emission intensity is used for the calculation of λ. Using the lateral intensity instead of the density is preferable as no Abel inversion is needed, thereby reducing the error in the calculations of λ.

The whole Fischer curve as shown in figure 4.2 was reproduced by determining λ from 1 to 10 g for lamps with different fillings and geometry, see figures 4.10 and 4.11. The lamps with a burner radius of 8 mm, a burner height of 20 mm and a Hg filling ranging from 5 mg to 10 mg, are predominantly on the right side of the Fischer curve (see figure 4.10). As g increases, the axial segregation parameter λ decreases, the experiments show that this decrease is proportional to $1/g$, which is consistent with theory. The lamp with a burner radius of 4 mm, a burner height of 22 mm and a Hg filling of 2.5 mg, are clearly on the left side of the curve (see figure 4.11) as the pressure is lower and the radius narrower. A lamp containing 0.73 mg of Hg, not shown in figure 4.11, shows an axial segregation parameter that is about a factor 10 less than the parameter found for the 2.5 mg Hg lamp. This is in agreement with equation 4.9. As g increases, the axial segregation parameter λ increases for the longer, thinner lamp, with no maximum occurring before 10 g.

After calibration with a ribbon lamp, the radial intensity profile of Hg was used to calculate the temperature profile numerically, as described in the section 4.2. Figure 4.12 shows temperature profiles from 4 g to 10 g near the bottom of the lamp. The axis temperature is about 6500 K at 10 g. The arc clearly contracts at high g-values due to the increase of convection. The lateral profiles near the bottom of the arc shown previously indicate that the amount of Dy decreases as g is increased. Dy is largely responsible for radiation loss and accompanied by contraction of the arc [3]. Despite the fact that the amount of Dy is decreasing, an increase of g still causes the contraction to increase. Apparently the convection predominates the radiation loss with regard to contraction at these high g-values. The contraction of the temperature profiles is also in agreement with the contraction as shown by the lateral profiles.

4.5 Conclusions

The whole Fischer curve was reproduced as the segregation parameter was determined for 1 to 10 g. The axial segregation parameter λ was calculated as a function of g from the atomic lateral profiles for lamps of different pressure and geometry. The experimental data follows the left and right side of the theoretical Fischer curve.

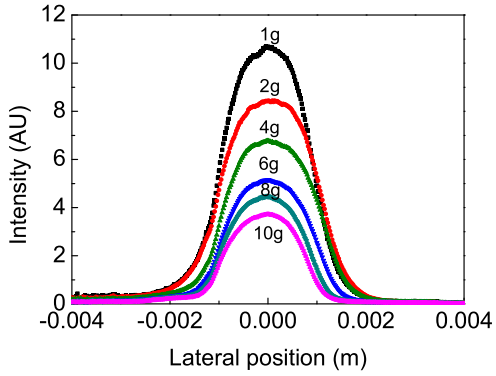

(a)

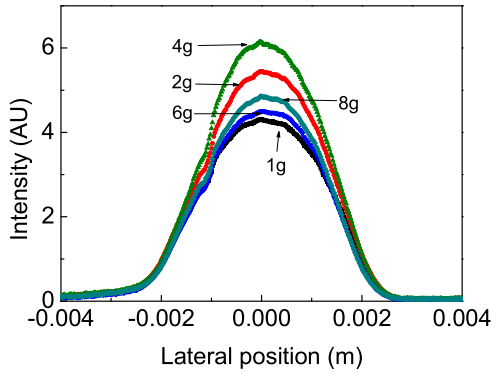

(b)

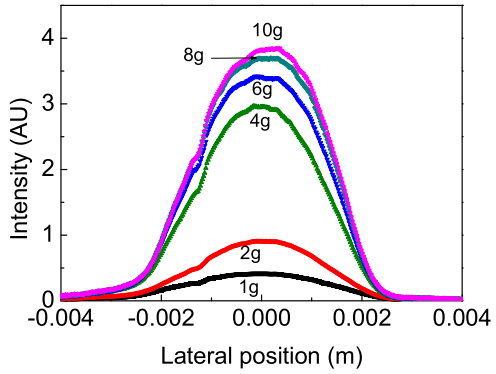

(c)

Figure 4.8: Ionic lateral profiles for the ionic line at 402.44 nm, The lamp filling was 10 mg Hg and 4 mg DyI_3 at three different axial positions. (a) near the bottom at z/Z=27,5%, (b) at the centre at z/Z=50%, (c) near the top at z/Z=72.5% where Z=20mm. Although the intensity was not calibrated, the measurements done at the same wavelength are absolute with respect to each other.

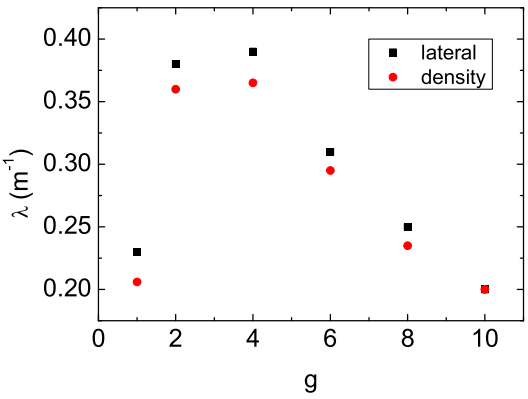

Figure 4.9: Fischer curve for a lamp containing 5 mg Hg 4 mg DyI_3 calculated using the lateral intensity profile and the radially resolved density profile.

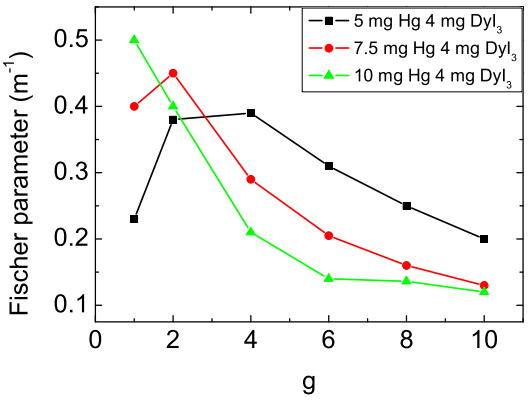

Figure 4.10: Fischer curve for lamps containing different Hg fillings, namely 5, 7.5 and 10 mg. In all cases DyI_3 = 4mg. Burner height is 20 mm and burner diameter is 8 mm.

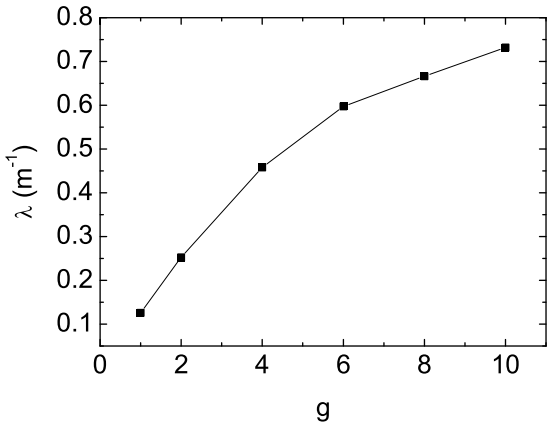

Figure 4.11: Fischer curve for a lamp containing 2.5 mg Hg and 2.5 mg DyI_3. Burner height is 22 mm and burner diameter is 4 mm.

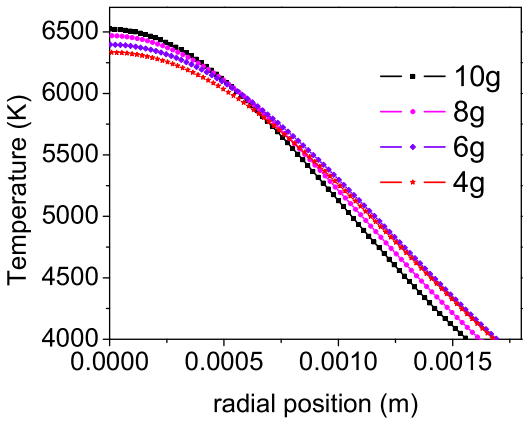

Figure 4.12: Radial temperature profile for a lamp containing 10mg Hg and 4 mg DyI_3 near the bottom, at the axial position of z/Z=27.5% of the lamp, where Z=20 mm.

Webcam pictures show that at higher g-values there is more mixing of the additives in the MH lamp due to an increase in convection. This is corroborated by atomic and ionic lateral profiles for lamps on the right side of the Fischer curve. The cold spot temperature decreases as g becomes higher. The increase of convection causes the arc to contract near the bottom of the lamp. Near the top of the lamp the arc broadens. Radial temperature profiles were determined from the Hg radial profiles for different g. Axis temperature at 10 g is about 6500 K. Contraction of the arc caused by convection predominates contraction caused by radiation loss near the bottom of the lamp.

Future work includes comparison of experimental results with a numerical model, the results provide excellent means for the testing of such a model.

4.6 Acknowledgements

T.N. acknowledges support from Technologiestichting STW (project ETF. 6093), ESA, NASA, COST (project 529), Senter Novem, SRON, the Dutch Ministries of Economic Affairs and Culture, Science and Education, Dutch Space, Verhaert, the executive board of the Eindhoven University of Technology and the Design and Engineering facilities of the Eindhoven University of Technology (GTD).

Bibliography

[1] Lister G G, Lawler J E, Lapatovich W P and Godyak V A 2004 Rev. Mod. Phys. **76**, 541

[2] Fischer E 1976 J. Appl. Phys. **47**, 2954

[3] Nimalasuriya T, Flikweert A J, Haverlag M, Kemps P C M, Kroesen G M W, Stoffels W W and Van der Mullen J J A M 2006 *J. Phys D: Appl Phys* **39** 2993 **see chapter 3**

[4] Flikweert A J, Van Kemenade M, Nimalasuriya T, Haverlag M, Kroesen G M W and Stoffels WW 2006 J.Phys.D **39**, 1599

[5] Stoffels W W, Haverlag M, Kemps P C M, Beckers J and Kroesen G M W 2005 Appl. Phys. Lett. **87** 1

[6] Nimalasuriya T, Pupat N B M, Flikweert A J, Stoffels W W, Haverlag M and Van der Mullen J J A M 2006 J. Appl. Phys. **99** 053302 **see chapter 2**

[7] Zhu X 2005 Ph.D. thesis *Active spectroscopy on HID lamps*, Eindhoven University of Technology

[8] Van der Mullen J J A M 1990 Phys. Rep. **191** 109

[9] Curry J J, Sakai M and Lawler J E 1998 J. Appl. Phys. **84**, 3066

[10] Kemps P C M, 2004 Master's thesis *An experimental study of the radial additive density and plasma temperature profiles, and the effect of this on the integral light output of metal halide lamps as a function of gravity* Eindhoven University of Technology

[11] Mitchner M and Kruger C H Jr 1973 *Partially ionized gases*,1st ed. (John Wiley and Sons).

[12] Kurucz R L and Bell B 1993 *Atomic Line Data CD-ROM No 23* (Cambridge, MA: Smithsonian Astrophysical Observatory)

[13] Wickliffe M W and Lawler J E 2000 J. Quant. Spectrosc. Radiat. Transfer **66**, 363

[14] `http://www.thespectroscopynet.com/Theory/Partition_Functions.asp`

[15] Fischer E 1978 *Influences of External and Self-Magnetic Fields on the behaviour of discharge lamps*, Philips GmbH Forschungslaboratorium Aachen Lobornotiz nr 13/78.

[16] Elenbaas W 1951 *The high pressure mercury vapour discharge*, 1st ed., (North-Holland publishing company)

[17] Benck E C, Lawler J E and Dakin J T 1989 J. Opt. Soc. Am. B **6**, 11

[18] Stoffels W W, Baede A H F M, Van der Mullen J J A M, Haverlag M and Zissis G 2006 Meas. Sci. Technol. **17**, N67

[19] Flikweert A J, Nimalasuriya T, Groothuis C H J M, Kroesen G M W and Stoffels W W 2005, J. Appl. Phys. **98** 073301